Auger Electron Radioimmunotherapeutic Agent Specific for the $CD123^+/CD131^-$ Phenotype of the Leukemia Stem Cell Population

Jeffrey Victor Leyton[1], Meiduo Hu[1], Catherine Gao[1], Patricia V. Turner[2], John E. Dick[3], Mark Minden[4,5], and Raymond M. Reilly[1,6,7]

[1]Department of Pharmaceutical Sciences, University of Toronto, Toronto, Ontario, Canada; [2]Department of Pathobiology, University of Guelph, Guelph, Ontario, Canada; [3]Department of Medical Genetics, University of Toronto, Toronto, Ontario, Canada; [4]Ontario Cancer Institute, University Health Network, Toronto, Ontario, Canada; [5]Department of Medical Biophysics, University of Toronto, Toronto, Ontario, Canada; [6]Department of Medical Imaging, University of Toronto, Toronto, Ontario, Canada; and [7]Toronto General Research Institute, University Health Network, Toronto, Ontario, Canada

Our aim was to construct and characterize ^{111}In-nuclear translocation sequence (NLS)-7G3, an Auger electron–emitting radioimmunotherapeutic agent that preferentially recognizes the expression of CD123 (interleukin-3 receptor [IL-3R] α-subchain) in the absence of CD131 (IL-3R β-subchain) displayed by leukemia stem cells. **Methods:** Monoclonal antibody 7G3 was modified with 13-mer peptides [CGYGPKKKRKVGG] harboring the NLS of SV-40 large T-antigen and with diethylenetriaminepentaacetic acid for labeling with ^{111}In. Immunoreactivity was evaluated in a competition radioligand binding assay and by flow cytometry. Nuclear localization of ^{111}In-NLS-7G3 was studied by cell fractionation in $CD123^+/CD131^-$ acute myelogenous leukemia (AML)-3, -4, and -5 cells or in primary AML or normal leukocytes. Micro-SPECT was performed in nonobese diabetic (NOD)/severe combined immune deficient (SCID) mice engrafted subcutaneously with Raji-CD123 tumors or with disseminated AML-3 or -5 cells. The cytotoxicity of ^{111}In-NLS-7G3 on AML-5 cells was studied after 7 d in culture by trypan blue dye exclusion. DNA damage was assessed using the γ-H2AX assay. **Results:** NLS-7G3 exhibited preserved CD123 immunoreactivity (affinity, 4.6 nmol/L). Nuclear importation of ^{111}In-NLS-7G3 in AML-3, -4, or -5 cells was specific and significantly higher than unmodified ^{111}In-7G3 and was greater in primary AML cells than in normal leukocytes. Rapid elimination of ^{111}In-NLS-7G3 in NOD/SCID mice prevented imaging of subcutaneous Raji-CD123 tumors. This phenomenon was Fc-dependent and IgG_{2a} isotype–specific and was overcome by the preadministration of excess IgG_{2a} or using ^{111}In-NLS-7G3 $F(ab')_2$ fragments. AML-3 and -5 cells were engrafted into the bone marrow or spleen or at extramedullary sites in NOD/SCID mice. Micro-SPECT/CT with ^{111}In-NLS-7G3 $F(ab')_2$ showed splenic involvement, whereas foci of disease were seen in the spine or femur or at extramedullary sites in the brain and lymph nodes using ^{111}In-NLS-7G3 IgG_{2a}. The viability of AML-5 cells was reduced by exposure in vitro to ^{111}In-NLS-7G3; this reduction was associated with an increase in unrepaired DNA double-strand breaks. **Conclusion:** ^{111}In-NLS-7G3 is a promising novel Auger electron–emitting radioimmunotherapeutic agent for AML aimed at the leukemia stem cell population. Micro-SPECT/CT was useful for visualizing the engraftment of leukemia in NOD/SCID mice.

Key Words: leukemia stem cells; Auger electrons; ^{111}In; radioimmunotherapy; micro-SPECT/CT

J Nucl Med 2011; 52:1465–1473
DOI: 10.2967/jnumed.111.087668

Acute myelogenous leukemia (AML) is thought to originate from a primitive malignant stem cell that shares the $CD34^+/CD38^-$ phenotype of normal hematopoietic stem cells (*1*). These leukemia stem cells (LSCs), discovered by Bonnet and Dick in 1997 (*2*), are present at a low frequency (<1%) but are resistant to cytotoxic therapy because of expression of multidrug resistance transporters (*3,4*). Consequently, despite the fact that remissions are induced in 60%–70% of patients by intensive chemotherapy combined with hematopoietic stem cell transplantation, only 1 in 5 AML patients survives more than 3 y (*5*). Therapeutic approaches that eradicate the LSC population would produce more durable remissions, and potentially cure (*1*). Our laboratory is exploring a novel radioimmunotherapeutic strategy to eradicate LSCs, which relies on the nanometer- to micrometer-range Auger electrons emitted by ^{111}In complexed to the anti-CD123 murine IgG_{2a} monoclonal antibody (mAb) 7G3. These electrons cause lethal DNA damage in cells, particularly if they are released near the nucleus (*6*). Jordan et al. reported that LSCs display the interleukin-3 receptor (IL-3R) α-subchain (CD123) in the absence of the β-chain, whereas normal hematopoietic stem cells display functional IL-3R (CD123/CD131) (*7*). mAb 7G3 is a murine IgG_{2a} that preferentially binds CD123 on AML blasts and LSCs with an affinity (K_d, 0.9 nM), which is 100-fold higher than IL-3 itself, whereas its

Received Jan. 8, 2011; revision accepted May 9, 2011.
For correspondence or reprints contact: Raymond M. Reilly, Leslie Dan Faculty of Pharmacy, University of Toronto, 144 College St., Toronto, ON, Canada M5S 3M2.
E-mail: raymond.reilly@utoronto.ca
Published online Aug. 4, 2011.

affinity for the functional IL-3R is 3-fold lower than that of IL-3 (*8*). mAb 7G3 is internalized after CD123 binding, which inserts ^{111}In into leukemia cells; to promote nuclear translocation, however, we modified 7G3 with peptides [CGYGPKKKRKVGG], which harbor the nuclear localization sequence (NLS) of SV-40 large T-antigen (underlined) (*9*). We report that ^{111}In-NLS-7G3 caused DNA double-strand breaks in vitro in CD123$^+$/CD131$^-$ AML cells, diminishing their viability when compared with untreated cells. In addition, we describe a practical and robust nonobese diabetic (NOD)/severe combined immune deficient (SCID) mouse model of AML established by engrafting leukemia cell lines that share the CD123$^+$/CD131$^-$ phenotype of LSCs. This model was instrumental in our ability to study tracking of ^{111}In-NLS-7G3 to sites of leukemia in the bone marrow (BM) and spleen or at other extramedullary (EM) sites. ^{111}In emits 2 highly abundant γ-photons (Eγ, 171 keV [90%] and 245 keV [94%]), in addition to the Auger electron emissions, that can be imaged by SPECT. Thus, high-spatial-resolution and high-sensitivity multipinhole micro-SPECT/CT was used to visualize the uptake of ^{111}In-NLS-7G3 at sites of leukemia in this model. Our results suggest that ^{111}In-NLS-7G3 is a promising radioimmunotherapeutic agent for eradication of the LSC population in AML. Moreover, micro-SPECT/CT with ^{111}In-NLS-7G3 permits assessment of dissemination of AML cells to survival niches in NOD/SCID mice.

MATERIALS AND METHODS

mAbs and Cells

Murine anti-CD123 mAb 7G3 and isotype-matched BM4 IgG_{2a} were provided by CSL Ltd. Murine IgG_1 was purchased from AbD Serotec. $F(ab')_2$ fragments were generated using immobilized pepsin-agarose beads (Pierce). Wild-type Raji cells and CD123-transfected clone (Raji-CD123) and Chinese hamster ovary (CHO)-CD123 cells were provided by CSL Ltd. AML lines 3, 4, and 5 were provided by Dr. Mark Minden (Ontario Cancer Institute) (*10*).

Radioimmunoconjugates

mAbs 7G3 and BM4 or $F(ab')_2$ fragments were modified with diethylenetriaminepentaacetic acid (DTPA) and NLS peptides [CGYGPKKKRKVGG] as previously reported (*11*). Approximately 100–300 μg of DTPA-NLS-mAbs or $F(ab')_2$ fragments in 1 M sodium acetate buffer, pH 6.0, were labeled with 74 MBq of $^{111}InCl_3$ (MDS-Nordion) at room temperature for 1 h. ^{111}In-labeled radioimmunoconjugates were purified on a Sephadex G-50 minicolumn (BioRad) eluted with phosphate-buffered saline, pH 7.4. The radiochemical purity was measured by instant thin-layer silica gel chromatography developed in 100 mM sodium citrate, pH 5.0, or by high-performance liquid chromatography on a Biosep SEC-S2000 column (Phenomenex Inc.).

Cell-Binding Assays

^{111}In-DTPA-7G3 (0.4 nM) was incubated for 1 h at 4°C with 1×10^5 CHO cells transfected with CD123 per well in a 24-well plate in the presence of 0.2–225 nM NLS-7G3 or 7G3. The K_d value was obtained by fitting the percentage ^{111}In bound versus log concentration of inhibitor (nmol/L). Flow cytometry was performed by incubating 1×10^5 Raji or Raji-CD123 cells in 100 μL of phosphate-buffered saline with 10 μg of nonlabeled NLS-7G3 or NLS-BM4 on ice for 30 min, rinsing, and following with 2 μL of phycoerythrin-conjugated antimouse Fc $F(ab')_2$ fragments for 30 min. Cells were counted (>10,000 events) in a flow cytometer (Beckman Coulter LSR II).

Nuclear Importation

The nuclear localization of ^{111}In-NLS-7G3 in AML cells, primary AML, and leukocytes from a healthy donor was measured at 2 h after incubation with the cells at 37°C by subcellular fractionation and compared with that of ^{111}In-NLS-BM4 or ^{111}In-7G3, as previously reported (*11*). Nuclear radioactivity was expressed as a percentage of ^{111}In added to cells in the wells.

Imaging of NOD/SCID Mice with Raji-CD123 Tumors

Raji-CD123 tumors were established by subcutaneous inoculation of 5×10^6 cells into NOD/SCID mice. Tumor-bearing mice were imaged using a NanoSPECT/CT (Bioscan) camera. Mice were injected intravenously (tail) with 20–30 μg (9.25–16.7 MBq) of ^{111}In-NLS-7G3 or ^{111}In-NLS-BM4 or 31–36 μg (7.4–17.7 MBq) of 7G3 or BM4 $F(ab')_2$. Some mice were preadministered a 5-fold excess of BM4 IgG_{2a} or 7G3 injected intraperitoneally at 12 h before radioimmunoconjugates. Tomographic images were obtained for a total of 50,000 counts per frame. Images were reconstructed using InVivo Scope software (version 1.40; Bioscan). Elimination of ^{111}In-NLS-7G3 or ^{111}In-labeled $F(ab')_2$ from the blood was determined after injection of 0.24–0.87 MBq (10 μg) in NOD/SCID or BALB/c mice. Blood samples were collected from the saphenous vein at 5, 15, and 30 min and at 1, 2, 3, 19, 24, 48, and 72 h after injection. The blood-radioactivity-versus-time curves were fitted to a 1-exponential decay, and the half-life ($t_{1/2}$) was estimated using Scientist software (version 2.01; Micromath). The radioactivity in blood, tumor, and normal organs was measured at 72 h after injection for ^{111}In-NLS-7G3 and at 48 h for $F(ab')_2$. All animal studies were approved by the Animal Care Committee at the University Health Network (protocol 864.5).

AML Cell Line Engraftment in NOD/SCID Mouse Model

AML-3, -4, or -5 cells sharing the CD123$^+$/CD131$^-$ phenotype of LSCs were engrafted into NOD/SCID mice. NOD/SCID mice received 300 cGy of γ-radiation 24 h before intravenous inoculation with 2–5 × 10^6 AML-3, -4, or -5 cells. Engraftment was determined by measuring the proportion of human cells in the BM and spleen and other EM sites by flow cytometry using allophycocyanin-antihuman CD45 antibodies (Beckman Coulter) at 26–46 d after cell inoculation, as previously reported (*12*). Further phenotypic characterization was performed using fluorescein isothiocyanate-anti-CD34, phycoerythrin-anti-CD123, phycoerythrin-anti-CD131 antibodies (BD Biosciences), and peridinin chlorophyll protein complex-antiCD38 antibodies (Biolegend). Hemoglobin, erythrocyte (red blood cells), leukocyte (white blood cells), and platelet counts were measured in a blood sample obtained by cardiac puncture.

Micro-SPECT/CT of AML Engraftment

Imaging studies were performed in NOD/SCID mice engrafted with AML-3 cells and injected with ^{111}In-NLS-7G3 $F(ab')_2$ or ^{111}In-NLS-7G3. Alternatively, NOD/SCID mice engrafted with AML-5 cells were injected with ^{111}In-NLS-7G3

with preadministration of BM4 IgG_{2a}. Western blotting for human CD45 on excised tissues from imaged mice was performed by electrophoresing 10 μg of tissue protein on a 4%–20% Tris HCl mini-gel (BioRad), transferring onto a nitrocellulose membrane (BioRad), and probing with goat antihuman CD45 mAbs (Serotec AbD). The immunoblot was developed with murine antigoat horseradish peroxidase–conjugated antibody (Serotec AbD) and imaged by chemiluminescence (Western Lightning; PerkinElmer).

DNA Damage and Cytotoxicity

DNA damage in AML-5 cells was evaluated using the γ-H2AX assay as previously reported (*13*). Approximately 5×10^6 AML-5 cells were incubated with 7.4 MBq (120 nM) of ^{111}In-NLS-7G3, ^{111}In-7G3, or unlabeled 7G3 (120 nM) for 24 h. The number of γ-H2AX foci per nucleus was calculated for each treatment in 3 microscopic fields. The cytotoxicity of ^{111}In-NLS-7G3 on AML-5 cells was determined by exposing 1×10^6 cells to 1 mL of growth medium alone, ^{111}In-NLS-7G3 (7.4 MBq, 120 nM), ^{111}In-acetate (7.4 MBq), or unlabeled 7G3 (120 nM) for 12 h. Cells were centrifuged at 420*g* for 5 min, and the supernatant was removed. Cells were then resuspended in 1 mL of fresh medium and cultured for 7 d. Cells were recovered and stained with 0.4% trypan blue (Sigma-Aldrich). The percentage cell viability was calculated by dividing the number of cells excluding trypan blue by the total number of cells counted. Comparisons were made to cells exposed to growth medium alone.

Statistical Analysis

Statistical significance in the nuclear translocation, pharmacokinetic, Raji-CD123 xenograft biodistribution, and cytotoxicity studies was determined using a 2-tailed Student *t* test ($P < 0.05$). For biodistribution studies in AML engraftment models, the nonparametric Mann–Whitney *U* test with a 1-tail *P* value ($P < 0.05$) or a 2-way ANOVA ($P < 0.05$) was used.

RESULTS

Radioimmunoconjugates

7G3 and BM4 mAbs were monofunctionalized with DTPA and NLS peptides as previously reported (*11*). NLS-7G3 and 7G3 competed for binding of ^{111}In-DTPA-7G3 to CD123-transfected CHO cells (K_d, 4.6 and 3.6 nmol/L, respectively; Supplemental Fig. 1A [supplemental materials are available online only at http://jnm.snmjournals.org]). Flow cytometry revealed binding of NLS-7G3 to CD123-transfected Raji cells but not to wild-type Raji cells (Supplemental Fig. 1B). NLS-BM4 did not bind to Raji-CD123 cells. 7G3 and NLS-7G3 were labeled with ^{111}In to a radiochemical purity greater than 95% and specific activity of 0.24–0.74 MBq/μg (3.60×10^7–1.11×10^8 GBq/mol).

Nuclear Importation

NLS modification of ^{111}In-7G3 achieved 14.7% ± 5.0%, 3.1% ± 2.2%, and 4.2% ± 3.6% importation into the nucleus of AML-3, -4, and -5 cells, respectively, at 2 h at 37°C (Fig. 1). In comparison to unmodified ^{111}In-7G3, NLS modification significantly increased nuclear radioactivity in AML-3, -4, and -5 cells ($P = 0.019$, 0.018, and 0.027, respectively). In primary AML cells, nuclear uptake of ^{111}In-NLS-7G3 was higher than ^{111}In-NLS-BM4 (20.9% ± 2.7% vs. 4.8% ± 4.0%; $P = 0.0045$; Supplemental Fig. 2). Moreover, there was lower uptake of ^{111}In-NLS-7G3 in the nucleus of leukocytes from a healthy donor (2.8% ± 0.7%; $P = 0.0004$) than in primary AML cells (Supplemental Fig. 2).

Imaging of NOD/SCID Mice with Raji-CD123 Tumors

Raji-CD123 tumors in NOD/SCID mice could not be visualized with ^{111}In-NLS-7G3 (Fig. 2A) at 24 h after injection. There was an unusually rapid elimination of ^{111}In-NLS-7G3 from the blood, with only 0.2 ± 0.1 percentage injected dose per gram (%ID/g) circulating at 72 h after injection (Table 1). The blood-concentration-versus-time curve for ^{111}In-NLS-7G3 was monoexponential, with a $t_{1/2}$ of 7.6 h (Fig. 2B; Supplemental Table 1). This rapid elimination in NOD/SCID was not present in BALB/c mice (5.0 ± 1.4 %ID/g in the blood at 72 h; $P = 0.002$). The $t_{1/2}$ for ^{111}In-NLS-7G3 in BALB/c mice (33.0 h) was longer than in NOD/SCID mice. In contrast, there was only a small difference in the $t_{1/2}$ of ^{111}In-NLS-7G3 F(ab′)$_2$ in NOD/SCID and BALB/c mice (6.1 vs. 5.9 h; Supplemental Fig. 3A and Supplemental Table 1). At 72 h after injection, there was 0.6 ± 0.2 %ID/g versus 0.9 ± 0.1 %ID/g in the blood of NOD/SCID or BALB/c mice ($P = 0.060$). Preadministration of a 10-fold excess of 7G3 at 24 h after ^{111}In-NLS-7G3 increased blood radioactivity at 72 h after injection (7.6 ± 1.7 %ID/g; Table 1) and increased the $t_{1/2}$ for ^{111}In-NLS-7G3 (17.8 h; Supplemental Table 1). Preadministration of BM4 increased uptake of ^{111}In-NLS-7G3 in Raji-CD123 tumors (14.7 ± 2.8 %ID/g; Table 1) allowing tumor visualization by micro-SPECT/CT (Fig. 2A). The CD123 dependence of tumor uptake of ^{111}In-NLS-7G3 was shown by lower uptake in wild-type Raji tumors

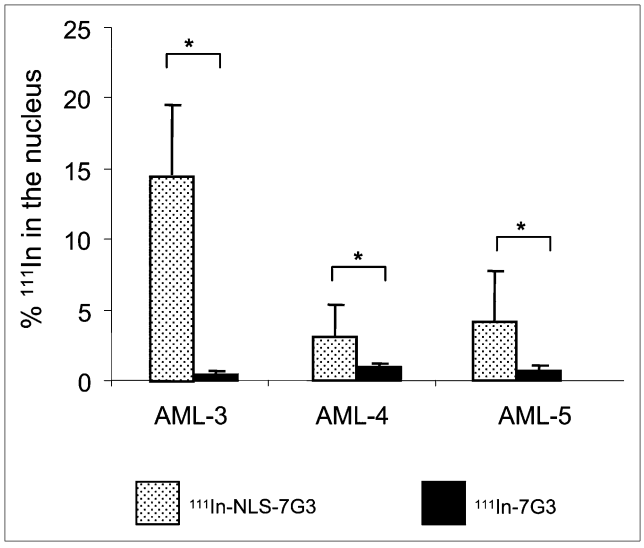

FIGURE 1. Percentage of nuclear radioactivity in AML-3, -4, or -5 cell lines incubated for 12 h at 37°C with ^{111}In-NLS-7G3 or ^{111}In-7G3. Significant differences ($P < 0.05$) are indicated by asterisks.

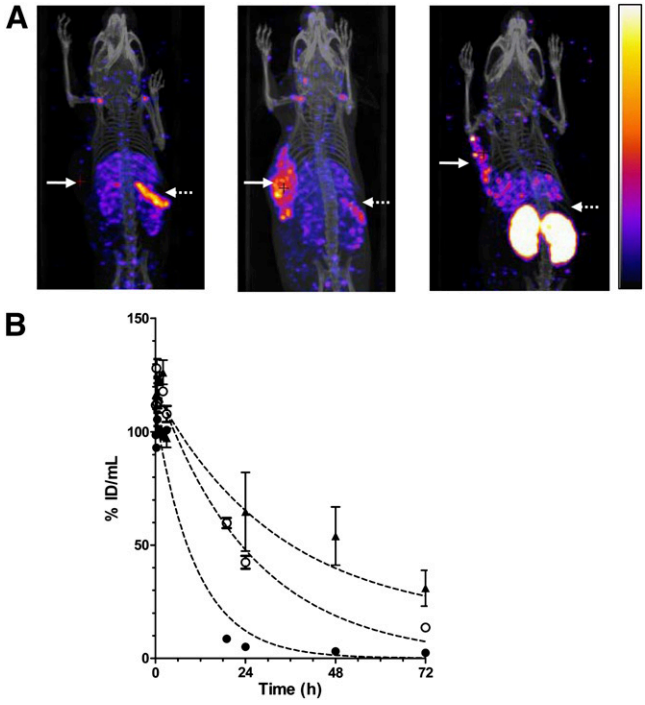

FIGURE 2. (A) Coronal micro-SPECT/CT images of subcutaneous Raji-CD123 xenografts (solid arrows) and spleen (broken arrows) in NOD/SCID mice injected with ^{111}In-NLS-7G3 (left image) at 24 h after injection, ^{111}In-NLS-7G3 with preadministration of BM4 IgG_{2a} at 72 h after injection (center image), or ^{111}In-NLS-7G3 F(ab′)$_2$ fragments at 48 h after injection (right image). Images were adjusted to equal intensity. (B) Elimination of radioactivity from blood after intravenous injection of ^{111}In-NLS-7G3 in NOD/SCID mice with (○) or without (●) preadministration of BM4 IgG_{2a} or in BALB/c mice without preadministration of BM4 (▲).

(2.1 ± 0.6 %ID/g; $P = 0.002$; Table 1). Preadministration of murine IgG_1 did not slow the elimination of ^{111}In-NLS-7G3 from the blood and did not permit imaging of Raji-CD123 tumors (Supplemental Fig. 3B). Raji-CD123 tumors were imaged with ^{111}In-NLS-7G3 F(ab′)$_2$ without preadministration of BM4 (Fig. 2A). The specificity of tumor uptake of ^{111}In-NLS-7G3 F(ab′)$_2$ was shown by the lower uptake of ^{111}In-NLS-BM4 F(ab′)$_2$ in Raji-CD123 tumors (7.2% ± 3.8% vs. 0.3% ± 0.1%; $P = 0.035$; Table 1). Normal spleen and kidneys were seen on images with ^{111}In-NLS-7G3 or the F(ab′)$_2$ fragments, respectively.

AML Cell Line Engraftment NOD/SCID Mouse Model

AML-3, -4, and -5 cells (all leukemia subtype M5) share the $CD123^+/CD131^-$ phenotype of LSCs and were engrafted into sublethally irradiated NOD/SCID mice. Gross examination showed spleen enlargement and BM whitening. Engraftment efficiencies based on the percentage of human $CD45^+$ cells were 12%, 0.5%, and 63% in the BM for AML-3, -4, and -5 cell lines, respectively (Supplemental Fig. 4A). Engraftment efficiency in the spleen was 26%, 20%, and 83% for AML-3, -4, and -5 cells, respectively. EM sites of leukemia were found in 2 of 5, 1 of 5, and 5 of 5 mice engrafted with AML-3, -4, or -5 cells. Most EM sites were in the brain parenchyma, spinal cord, or lymph nodes (LNs) and harbored 100% $CD45^+$ cells. Histopathologic examination revealed infiltration of leukemia cells into the ocular nerve, brain, and a mandibular LN (Supplemental Figs. 4B–4D). AML-engrafted mice exhibited lower hemoglobin, red blood cell, and platelet counts and higher white blood cell counts than did healthy nonirradiated or irradiated NOD/SCID mice (Supplemental Figs. 4E–4H).

Imaging Leukemia Uptake of ^{111}In-NLS-7G3 F(ab′)$_2$ in AML-3–Engrafted Mice

Biodistribution studies revealed that there was higher mean uptake of ^{111}In-NLS-7G3 F(ab′)$_2$ than ^{111}In-NLS-BM4 F(ab′)$_2$ in the spleen of AML-3–engrafted mice (Fig. 3A), although it did not reach statistical significance possibly because of variable AML engraftment. In 2 representative AML-3–engrafted mice, the spleen was visualized by micro-SPECT/CT with ^{111}In-NLS-7G3 F(ab′)$_2$ (Fig. 3B), but in a representative mouse receiving ^{111}In-NLS-BM4 F(ab′)$_2$ the spleen was not seen (Fig. 3B). Possible EM sites of leukemia were imaged in the orbit of the eye and in an LN in 1 mouse receiving ^{111}In-NLS-7G3 F(ab′)$_2$ (Fig. 3B). Mean uptake of ^{111}In-NLS-7G3 F(ab′)$_2$ in the femur including the BM (a site of leukemia) was significantly ($P = 0.047$) higher than ^{111}In-NLS-BM4 F(ab′)$_2$ (Fig. 3A). At 48 h after injection, biodistribution studies (Table 2) revealed significantly greater uptake of ^{111}In-NLS-7G3 F(ab′)$_2$ than ^{111}In-NLS-BM4 F(ab′)$_2$ in the liver ($P = 0.045$) and kidneys ($P = 0.047$).

Imaging Leukemia Uptake of ^{111}In-NLS-7G3 in AML-3–Engrafted Mice

There was significantly greater uptake of ^{111}In-NLS-7G3 into the spleen ($P = 0.0037$) and femur (including the BM; $P = 0.0237$) of AML-3–engrafted NOD/SCID mice than nonengrafted (nonirradiated or irradiated) NOD/SCID mice at 72 h after injection (Fig. 4A; Table 2). The mean uptake of ^{111}In-NLS-7G3 in the femur and spleen of nonirradiated and nonengrafted NOD/SCID mice was 3.8 ± 0.6 %ID/g and 38.1 ± 2.5 %ID/g, respectively. The radioactivity in the blood of AML-3–engrafted mice injected with ^{111}In-NLS-7G3 was significantly higher ($P = 0.0015$) than in either nonengrafted group. In 3 representative AML-3–engrafted mice, multiple small foci of radioactivity were imaged in the spine, pelvis, and femur (Fig. 4B). EM leukemia deposits were imaged. Human $CD45^+$ cells in the BM and spleen and at EM sites were detected by Western blotting or immunohistochemistry (Supplemental Fig. 5).

Imaging Leukemia Uptake in AML-5–Engrafted Mice

In NOD/SCID mice engrafted with AML-5 cells, preadministration of a 5-fold excess of BM4 24 h before ^{111}In-NLS-7G3 resulted in higher femoral uptake (including the BM) than ^{111}In-NLS-BM4 (Fig. 5A; Table 2; $P = 0.0159$). Mean AML-5 engraftment efficiencies in the BM were 52.9% and 43.0% in mice receiving ^{111}In-NLS-7G3 or

TABLE 1
Biodistribution of ^{111}In-NLS-7G3 and ^{111}In-NLS-BM4 mAbs or F(ab′)$_2$ Fragments in NOD/SCID Mice Implanted Subcutaneously with CD123-Transfected Raji or Nontransfected Raji Tumor Xenografts

Organ	Without IgG_{2a} preadministration		^{111}In-NLS-7G3 with IgG_{2a} preadministration		F(ab′)$_2$ fragments	
	^{111}In-NLS-7G3	^{111}In-NLS-BM4	BM4 excess	7G3 excess	^{111}In-NLS-7G3	^{111}In-NLS-BM4
Blood	0.2 ± 0.1	0.2 ± 0.1	4.0 ± 1.0*	7.6 ± 1.7*	1.4 ± 0.8†	0.6 ± 0.1
Liver	4.0 ± 2.3	2.0 ± 0.1	7.3 ± 1.0	8.0 ± 0.5	3.5 ± 1.9	1.3 ± 0.4
Spleen	35.4 ± 13.9	31.6 ± 2.4	27.0 ± 4.1	36.1 ± 3.9	5.0 ± 4.6	11.0 ± 0.2
Kidneys	6.2 ± 1.7	4.9 ± 0.5	9.4 ± 1.0	12.0 ± 0.6	9.6 ± 2.4	13.7 ± 4.4
Muscle	1.0 ± 0.9	1.0 ± 0.2	0.9 ± 0.3	1.0 ± 0.2	1.0 ± 0.4	0.6 ± 0.1
Raji-CD123	1.4 ± 0.5	0.7 ± 0.4	14.7 ± 2.8*,‡	5.5 ± 3.1*	7.2 ± 3.8†	0.3 ± 0.1
Raji	ND	ND	2.1 ± 0.6	ND	ND	ND

*Significantly different ($P < 0.05$), compared with ^{111}In-NLS-7G3 or ^{111}In-NLS-BM4 without preadministration of excess IgG_{2a}.
†Significantly different ($P < 0.05$), compared with ^{111}In-NLS-7G3 and ^{111}In-NLS-BM4 F(ab′)$_2$.
‡Significantly different ($P < 0.05$), compared with nontransfected Raji tumors.
Data are %ID/g (mean ± SD).
ND = Not determined.
Results were obtained at 72 h after injection for intact IgG_{2a} and at 48 h after injection for F(ab′)$_2$ fragments.

^{111}In-NLS-BM4 ($P = 0.443$; Fig. 5A). A representative photograph (Fig. 5B) depicts AML growth at an epiphyseal region in the femur also seen on CT (Fig. 5B). Imaging demonstrated uptake of ^{111}In-NLS-7G3 in these regions (Fig. 5B), compared with a mouse injected with ^{111}In-NLS-BM4 (Fig. 5C).

DNA Damage and Cytotoxicity

The viability of 1×10^6 AML-5 cells exposed to ^{111}In-NLS-7G3 and cultured for 7 d was diminished by ^{111}In-NLS-7G3, compared with cells exposed to growth medium alone (Fig. 6A). There was no significant effect on the viability of AML-5 cells exposed to noninternalized ^{111}In-acetate or unlabeled 7G3 (Fig. 6A). AML-5 cells exposed to ^{111}In-NLS-7G3 showed an increase in γ-H2AX foci representing unrepaired DNA double-strand breaks in the nucleus (4.8 ± 0.2 foci per nucleus; Fig. 6B), compared with cells exposed to growth medium (0.2 ± 0.3 foci per nucleus; Fig. 6 E; $P = 0.0001$). Cells exposed to ^{111}In-7G3 also exhibited an increase in γ-H2AX foci (3.0 ± 0.9 foci per nucleus; Fig. 6C; $P = 0.006$), compared with medium-exposed cells. There appeared to be a higher number of γ-H2AX foci in cells treated with unlabeled 7G3 (2.6 ± 1.5; Fig. 6D), compared with cells exposed only to medium, but this difference was not significant ($P = 0.06$).

DISCUSSION

Our results showed that ^{111}In-NLS-7G3 was imported in vitro into the nucleus of AML-3, -4, and -5 cells that share the CD123$^+$/CD131$^-$ phenotype of LSCs, as well as in primary human AML cells. The release of nanometer- to micrometer-range Auger electrons by ^{111}In-NLS-7G3 in AML-5 cells near DNA caused double-strand breaks that diminished their viability. Furthermore, micro-SPECT/CT showed that ^{111}In-NLS-7G3 specifically tracked to known sites of AML engraftment in the spleen and BM as well as into EM sites (brain and LNs) in NOD/SCID mice. Specific uptake of ^{111}In-NLS-7G3 and its F(ab′)$_2$ fragments was also demonstrated in NOD/SCID mice engrafted subcutaneously with Raji-CD123 tumors. Although these results

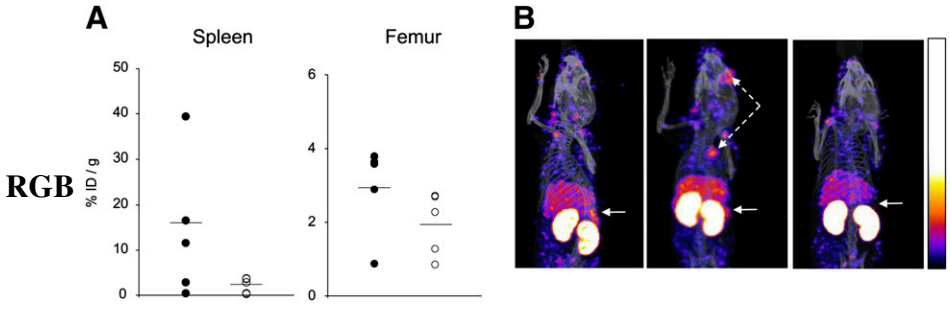

FIGURE 3. (A) %ID/g in spleen and femur in NOD/SCID mice engrafted with AML-3 cells at 48 h after injection with ^{111}In-NLS-7G3 F(ab′)$_2$ (●) or ^{111}In-NLS-BM4 F(ab′)$_2$ (○). Mean values are indicated by horizontal lines. (B) Coronal micro-SPECT/CT images of AML-3–engrafted NOD/SCID mice at 48 h after injection of ^{111}In-NLS-7G3 F(ab′)$_2$ (left and center images) or ^{111}In-NLS-BM4 F(ab′)$_2$ (right image). EM sites of radioactivity uptake in brain and LNs (broken arrows) are noted in center image, and spleen (solid arrow) is visualized in left and center images but not in right image. Images were adjusted to equal intensity.

TABLE 2
Biodistribution of ^{111}In-NLS-7G3 and ^{111}In-NLS-BM4 mAbs or ^{111}In-NLS-F(ab′)$_2$ Fragments in AML Engrafted NOD/SCID Mice

	AML-3				AML-5	
Engraftment	^{111}In-NLS-7G3-F(ab′)$_2$	^{111}In-NLS-BM4-F(ab′)$_2$	^{111}In-NLS-7G3 + AML	^{111}In-NLS-7G3 no AML	BM4 predose + ^{111}In-NLS-7G3	BM4 predose + ^{111}In-NLS-BM4
Blood	2.0 ± 1.2	1.2 ± 0.6	1.7 ± 0.2*	0.4 ± 0.2	2.4 ± 1.8	4.4 ± 2.7
Liver	4.9 ± 1.8†	2.0 ± 0.1	6.6 ± 1.4	6.5 ± 1.9	4.6 ± 2.2	4.6 ± 3.0
Spleen	17.6 ± 15.6	2.1 ± 1.7	62.8 ± 2.2*	32.3 ± 6.6	17.4 ± 2.6	18.0 ± 2.7
Kidneys	16.9 ± 6.3†	10.2 ± 2.2	10.3 ± 3.5	5.9 ± 1.5	6.6 ± 2.6	10.5 ± 2.8
Femur and BM	3.3 ± 0.4†	2.0 ± 0.9	9.2 ± 2.4*	3.1 ± 1.3	17.3 ± 10.3†	5.7 ± 4.2

*Significantly different ($P < 0.05$), compared with irradiated and nonengrafted NOD/SCID mice.
†Significantly different ($P < 0.05$), compared with isotype control.
Data are %ID/g (mean ± SD). Results were obtained at 72 h after injection for intact IgG_{2a} and at 48 h after injection for F(ab′)$_2$ fragments.

are promising for further study of ^{111}In-NLS-7G3 for Auger electron radioimmunotherapy of AML, they additionally show that CD123-targeted AML engraftment in NOD/SCID mice can be visualized by micro-SPECT/CT. At present, AML engraftment is routinely assessed in NOD/SCID mice by sacrificing the mice and determining the proportion of human cells ex vivo in the BM or spleen by flow cytometry. This does not permit longitudinal monitoring of individual mice to evaluate the kinetics of engraftment or to study the effects of treatment on the leukemic burden and, especially, to identify recurrence after treatment, which is the major challenge in treating AML in humans (*5*).

Micro-SPECT/CT revealed a pharmacokinetic barrier that prevented effective delivery of ^{111}In-NLS-7G3 to Raji-CD123 xenografts that was IgG_{2a}-specific and Fc-mediated. The rapid elimination of ^{111}In-NLS-7G3 in NOD/SCID mice but not in BALB/c mice was most likely due to low levels of circulating IgG_{2a} which previously caused sequestration of mAbs of this isotype by FcγRI receptors in the liver and spleen (*14*). Here, we report this phenomenon in NOD/SCID mice and emphasize its importance for evaluating 7G3 (and other IgG_{2a} mAbs) for treatment of AML in this model. Jin et al. found that treatment of NOD/SCID mice with unlabeled 7G3 at 6 h after inoculation of AML cells abrogated engraftment, whereas treatment at 24 h was less effective, and treatment at 28 d decreased the leukemic burden in only 2 of 5 groups of mice (*12*). These results imply that administration of 7G3 shortly after cell inoculation provided the greatest access to circulating LSCs and minimized the effects of sequestration by the spleen. In contrast, the effectiveness of 7G3 in mice

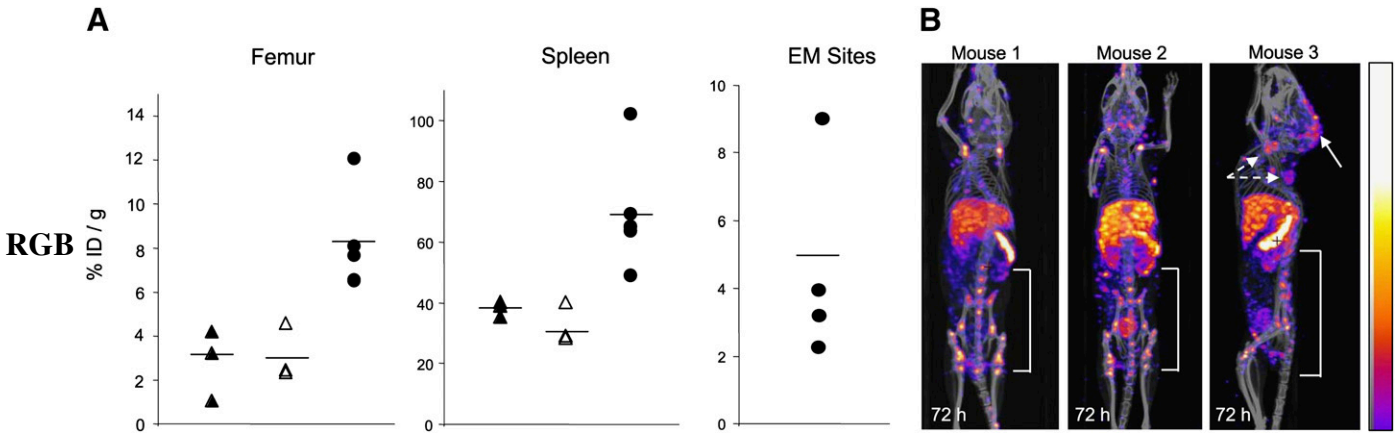

FIGURE 4. (A) %ID/g in femur, spleen, or EM sites at 72 h after injection of ^{111}In-NLS-7G3 in nonengrafted and nonirradiated (▲), nonengrafted and irradiated (△), and AML-3–engrafted and irradiated NOD/SCID mice (●). Mean values are indicated by horizontal lines. (B) Micro-SPECT/CT images of AML-3 engrafted NOD/SCID mice at 72 h after injection of ^{111}In-NLS-7G3 showing uptake in femur, pelvis, and spine. Mouse 3 is shown in sagittal projection to show EM sites of uptake in LNs (broken arrows) and brain parenchyma (solid arrow). Images were adjusted to equal intensity.

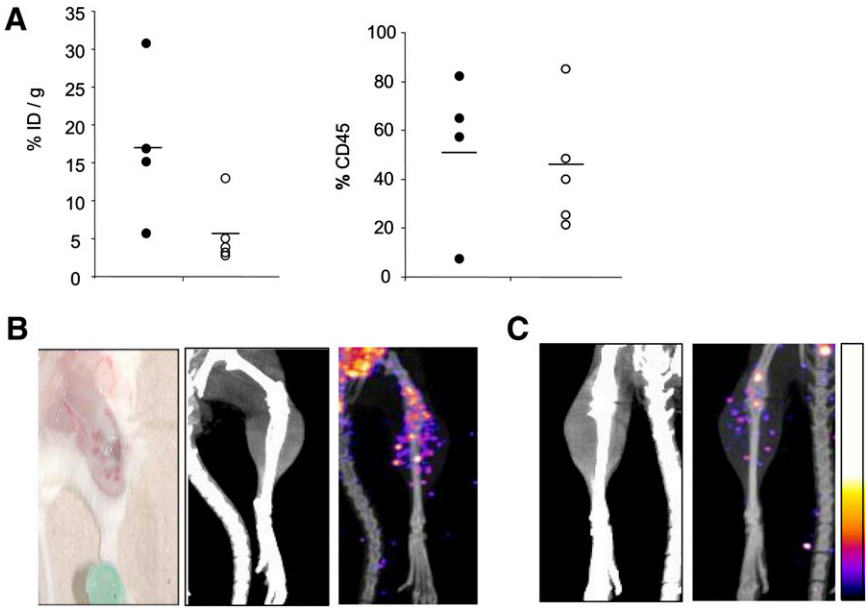

FIGURE 5. (A) On left is shown %ID/g in AML-5–engrafted NOD/SCID mice at 72 h after injection with ^{111}In-NLS-7G3 (●) or ^{111}In-NLS-BM4 (○). On right is shown percentage human CD45^{+} cells in AML-5–engrafted NOD/SCID mice receiving ^{111}In-NLS-7G3 (●) or ^{111}In-NLS-BM4 (○). (B) Photograph showing epiphysial leukemia outgrowth in femur in mouse receiving ^{111}In-NLS-7G3 (left), corresponding CT image (center), and micro-SPECT/CT image (right) showing radioactivity uptake into femoral leukemia outgrowth. (C) CT image of femoral leukemia outgrowth in mouse injected with ^{111}In-NLS-BM4 (left) and corresponding micro-SPECT/CT image of radioactivity uptake (right). Images were adjusted to same intensity.

with established leukemia could be reduced by uptake in the liver and spleen before reaching leukemia cells in the BM. In our study, preadministration of an excess of irrelevant BM4 IgG_{2a} slowed the elimination of ^{111}In-NLS-7G3 and greatly increased uptake into Raji-CD123 tumors. Normal-organ sequestration of radiolabeled mAbs is an important consideration in humans, and analogous preloading strategies have proven effective for decreasing liver uptake and promoting the BM accumulation of ^{111}In-labeled YAML568 anti-CD45 IgG_{2a} mAbs in patients with AML (*15*). Increased BM uptake was associated with complete remission in 4 patients undergoing hematopoietic stem cell transplantation in which ^{90}Y-labeled YAML568 was used in the conditioning regimen. Others have also found rapid elimination of radiolabeled mAbs that diminished their effectiveness for BM conditioning in AML (*16,17*).

Despite the antileukemic effects of unlabeled 7G3 in NOD/SCID mice (*12*), a phase I trial of CSL360, a chimeric IgG_1 analog of 7G3, reported only 1 complete response among 26 patients with relapsed, refractory, or high-risk AML treated at doses of 0.1–10 mg/kg (*18*). Combining 7G3 or CSL360 mAbs with ^{111}In and our nuclear localization strategy may improve their effectiveness. We previously reported that ^{111}In-NLS-HuM195 anti-CD33 mAbs killed HL-60 leukemia cells and retained their cytotoxicity toward HL-60/MX-1 cells with mitoxantrone resistance or primary AML specimens with multidrug resistance phenotype (*19*). This finding suggests that multidrug resistance transporter expression, which is a characteristic of LSCs (*3,4*), may not be an impediment to treatment with ^{111}In-labeled mAbs. A challenge for radioimmunotherapy of AML with ^{111}In-NLS-7G3, however, is low CD123

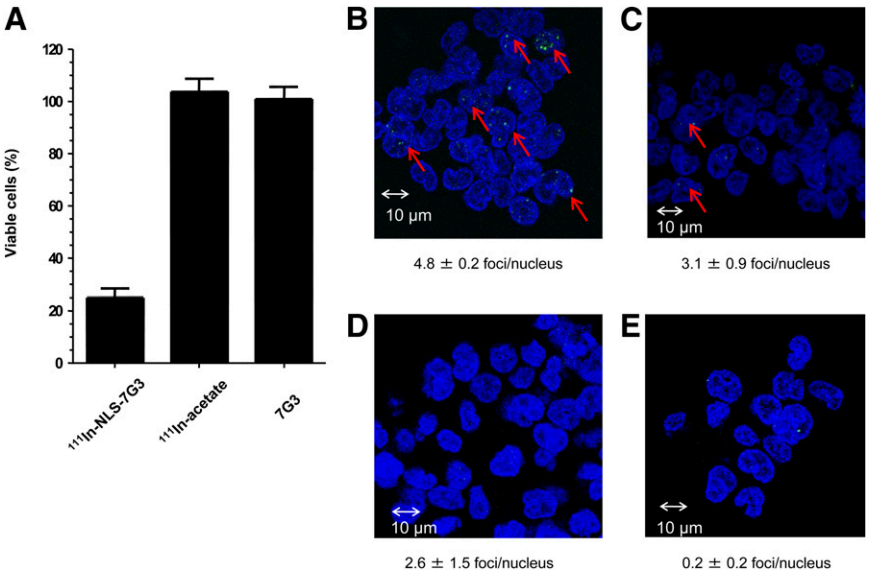

FIGURE 6. (A) Percentage of viable AML-5 cells after exposure for 12 h to 120 nM ^{111}In-NLS-7G3 (0.4 MBq/µg), equivalent amount of ^{111}In acetate, or unlabeled 7G3 (120 nM) and culturing for 7 d. Results of γ-H2AX assays probing unrepaired DNA double-strand breaks (bright foci and red arrows) in AML-5 cells exposed to ^{111}In-NLS-7G3 (B), ^{111}In-7G3 (C), unlabeled 7G3 (D), or growth medium alone (E). Number of γ-H2AX foci per nucleus (counterstained blue with 4′,6-diamidino-2-phenylindole) is shown.

expression (4×10^4 sites per cell) (*20*), possibly explaining the inability in our study to diminish the viability of AML-5 cells by more than 4-fold using ^{111}In-NLS-7G3 with relatively low specific activity (0.24–0.74 MBq/μg). An analogous effect was found for ^{111}In-NLS-HuM195 on $CD33^+$ leukemia cells in which a minimum specific activity of 2 MBq/μg was needed for cytotoxicity (*19*). Strategies to increase the specific activity of ^{111}In-NLS-7G3 by conjugation to starburst polyamidoamine dendrimers that permit conjugation to large numbers of DTPA chelators for complexing ^{111}In may enhance its effectiveness (*21*).

Finally, another contribution of our study was the establishment and characterization of a NOD/SCID mouse model that used AML-3, -4, or -5 cell lines that share the $CD123^+/CD131^-$ phenotype of LSCs but can be easily maintained in culture. Engraftment of primary AML specimens into the BM and spleen of NOD/SCID mice is a standard model of the disease (*22*), but there is high variability in engraftment efficiency (*23–27*). Furthermore, the proportion of $CD123^+$ cells varies between specimens, and cells from a single specimen cannot be easily expanded in culture to inoculate groups of mice with AML cells that have a predefined level of CD123. Therefore, the establishment of this more practical NOD/SCID mouse model of AML using these cell lines was instrumental in our ability to evaluate the delivery of ^{111}In-NLS-7G3 and its $F(ab')_2$ fragments to leukemia in the BM and spleen and at EM sites.

CONCLUSION

^{111}In-NLS-7G3 was specifically bound, internalized, and translocated to the nucleus of AML cells displaying the $CD123^+/CD131^-$ phenotype of LSCs. Emission of nanometer to micrometer Auger electrons near DNA caused double-strand breaks, reducing the viability of AML cells. ^{111}In-NLS-7G3 and its $F(ab')_2$ fragments specifically localized in subcutaneous Raji-CD123 tumor xenografts as well as at sites of leukemia in the BM and spleen or at other EM sites in NOD/SCID mice. These results are promising for further study of ^{111}In-NLS-7G3 for treatment of AML.

DISCLOSURE STATEMENT

The costs of publication of this article were defrayed in part by the payment of page charges. Therefore, and solely to indicate this fact, this article is hereby marked "advertisement" in accordance with 18 USC section 1734.

ACKNOWLEDGMENTS

We are grateful for the expert advice of Dr. Gino Vairo and Dr. Samantha Busfield at CSL Ltd., Parkville, Australia. We thank Dr. David Green and Doug Vines for suggestions on micro-SPECT/CT; Dr. Humphrey Fonge, Dr. Conrad Chan, Dr. Liqing Jin, Andreas Poeppl, Dr. Haytham Khoury, Vicky Cui, Dr. Alyssa Goldstein, and Deborah Scollard for technical assistance; and Matthew Dirk for assistance with pharmacokinetic fitting. This study was supported by a grant from the Canadian Institutes of Health Research (MOP 82886). No other potential conflict of interest relevant to this article was reported.

REFERENCES

1. Lane SW, Scadden DT, Gilliland DG. The leukemic stem cell niche: current concepts and therapeutic opportunities. *Blood.* 2009;114:1150–1157.
2. Bonnet D, Dick JE. Human acute myeloid leukemia is organized as a hierarchy that originates from a primitive hematopoietic cell. *Nat Med.* 1997;3:730–737.
3. Ishikawa F, Yoshida S, Saito Y, et al. Chemotherapy-resistant human AML stem cells home to and engraft within the bone-marrow endosteal region. *Nat Biotechnol.* 2007;25:1315–1321.
4. Wulf G, Wang R-Y, Kuehnle I, et al. A leukemic stem cell with intrinsic drug efflux capacity in acute myeloid leukemia. *Blood.* 2001;98:1166–1173.
5. Shipley JL, Butera JN. Acute myelogenous leukemia. *Exp Hematol.* 2009;37:649–658.
6. Reilly RM, Kassis A. Targeted Auger electron radiotherapy of malignancies. In: Reilly RM, ed. *Monoclonal Antibody and Peptide-Targeted Radiotherapy of Cancer.* Hoboken, NJ: John Wiley & Sons, Inc.; 2010:289–348.
7. Jordan CT, Upchurch D, Szilvassy SJ, et al. The interleukin-3 receptor alpha chain is a unique marker for human acute myelogenous leukemia stem cells. *Leukemia.* 2000;14:1777–1784.
8. Sun Q, Woodcock JM, Rapoport A, et al. Monoclonal antibody 7G3 recognizes the N-terminal domain of the human interleukin-3 (IL-3) receptor α-chain and functions as a specific IL-3 receptor antagonist. *Blood.* 1996;87:83–92.
9. Costantini DL, Hu M, Reilly RM. Peptide motifs for insertion of radiolabeled biomolecules into cells and routing to the nucleus for cancer imaging or radiotherapeutic applications. *Cancer Biother Radiopharm.* 2008;23:3–24.
10. Cencic R, Carrier M, Trnkus A, Porco Jr. JA, Minden M, Pelletier J. Synergistic effect of inhibiting translation initiation in combination with cytotoxic agents in myelogenous leukemia cells. *Leukemia Res.* 2010;34:535–541.
11. Chen P, Wang J, Hope K, et al. Nuclear localizing sequences (NLS) promote nuclear translocation and enhance the radiotoxicity of the anti-CD33 monoclonal antibody HuM195 labeled with ^{111}In in human myeloid leukemia cells. *J Nucl Med.* 2006;47:827–836.
12. Jin L, Lee EM, Ramshaw HS, et al. Monoclonal antibody-mediated targeting of CD123, IL-3 receptor α chain, eliminates human acute myeloid leukemic stem cells. *Cell Stem Cell.* 2009;5:31–42.
13. Cai Z, Chen Z, Bailey KE, Scollard DA, Reilly RM, Vallis KA. Relationship between induction of phosphorylated H2AX and survival in breast cancer cells exposed to ^{111}In-DTPA-hEGF. *J Nucl Med.* 2008;49:1353–1361.
14. Michel RB, Ochakovskaya R, Mattes MJ. Rapid blood clearance of injected mouse IgG2a in SCID mice. *Cancer Immunol Immunother.* 2002;51:547–556.
15. Glatting G, Müller M, Koop B, et al. Anti-CD45 monoclonal antibody YAML568: a promising radioimmunoconjugate for targeted therapy of acute leukemia. *J Nucl Med.* 2006;47:1335–1341.
16. Burke JM, Caron PC, Papadopolous EB, et al. Cytoreduction with iodine-131-anti-CD33 antibodies before bone marrow transplantation for advanced myeloid leukemias. *Bone Marrow Transplant.* 2003;32:549–556.
17. Kotzerke J, Glatting G, Seitz U, et al. Radioimmunotherapy for the intensification of conditioning before stem cell transplantation: differences in dosimetry and biokinetics of ^{188}Re- and ^{99m}Tc-labeled anti-NCA-95 Mabs. *J Nucl Med.* 2000;41:531–537.
18. Roberts AW, He S, Bradstock KF, et al. A phase 1 and correlative biological study of CSL360 (anti-CD123 mAb) in AML. Paper presented at: Proceedings of the 50th Annual Meeting American Society of Hematology; December 6–9, 2008; San Francisco, CA.
19. Kersemans V, Cornelissen B, Minden M, Brandwein J, Reilly RM. Drug-resistant AML cells and primary AML specimens are killed by ^{111}In-anti-CD33 monoclonal antibodies modified with nuclear localizaing peptide sequences. *J Nucl Med.* 2008;49:1546–1554.
20. Du X, Ho M, Pastan I. New immunotoxins targeting CD123, a stem cell antigen on acute myeloid leukemia cells. *J Immunother.* 2007;30:607–613.
21. Wängler C, Moldenhauer G, Eisenhut M, Haberkorn U, Mier W. Antibody-dendrimer conjugates: the number, not the size of the dendrimers, determines the immunoreactivity. *Bioconjug Chem.* 2008;19:813–820.

22. McCormack E, Bruserud O, Gjertsen BT. Animal models of acute myelogenous leukemia: development, application and future perspectives. *Leukemia.* 2005;19: 687–706.
23. Agliano A, Martin-Padura I, Mancuso P, et al. Human acute leukemia cells injected in NOD/LtSz-*scid*/IL-2Rγ null mice generate a faster and more efficient disease compared to other NOD/*scid*-related strains. *Int J Cancer.* 2008;123: 2222–2227.
24. Ailles LE, Gerhard B, Kawagoe H, Hogge DE. Growth characteristics of acute myelogenous leukemia progenitors that initiate malignant hematopoiesis in nonobese diabetic/severe combined immunodeficient mice. *Blood.* 1999;94:1761–1772.
25. Bonnet D, Bhatia M, Wang JYC, Kapp U, Dick JE. Cytokine treatment or accessory cells are required to initiate engraftment of purified primitive human hematopoietic cells transplanted at limiting doses into NOD/SCID mice. *Bone Marrow Transplant.* 1999;23:203–209.
26. Pearce DJ, Taussig D, Zibara K, et al. AML engraftment in the NOD/SCID assay reflects the outcome of AML: implications for our understanding of the heterogeneity of AML. *Blood.* 2006;107:1166–1173.
27. Taussig DC, Pearce DJ, Simpson C, et al. Hematopoietic stem cells express multiple myeloid markers: implications for the origin and targeted therapy of acute myeloid leukemia. *Blood.* 2005;106:4086–4092.